Journal of Materials Chemistry A

Accepted Manuscript

ROYAL SOCIETY OF CHEMISTRY

www.rsc.org/materialsA

Cite this: DOI: 10.1039/ c1ee00000x

www.rsc.org/ees

PAPER

In Situ Growth of CuS and $Cu_{1.8}S$ Nanosheet Arrays as Efficient Counter Electrodes for Quantum Dot-Sensitized Solar Cells

Meidan Ye,[a] Xiaoru Wen,[b] Nan Zhang,[b] Wenxi Guo,[a] Xiangyang Liu,[a] Changjian Lin*[ab]

Received (in XXX, XXX) Xth XXXXXXXXX 20XX, Accepted Xth XXXXXXXXX 20XX

DOI: 10.1039/c1ee00000x

Vertical CuS nanosheet arrays were firstly synthesized in situ on transparent conducting fluorine-doped tin oxide (FTO) substrates via a facile solvothermal process of seeded FTO glasses in the presence of ethanol solvent only containing thiourea and $Cu(NO_3)_2$ as precursor. While choosing CuCl instead of $Cu(NO_3)_2$ as the copper precursor in the same solvothermal process, porous $Cu_{1.8}S$ nanosheets, for the first time, were also vertically grown on FTO substrates, suggesting that such synthesis process is a general approach for the preparation of copper sulfide nanosheet arrays. When served as the low-cost counter electrode materials in quantum dot-sensitized solar cells (QDSSCs), CuS (3.95%) and $Cu_{1.8}S$ (3.30%) nanosheet films exhibited enhanced power conversion efficiencies in comparison with the conventional Pt film (1.99%), which was primarily due to the excellent electrocatalytic activity of copper sulfides for the reduction of polysulfide electrolyte used in CdSe/CdS QDSSCs. Significantly, the in situ growth strategy largely simplified the fabrication procedure of copper sulfide counter electrodes, meanwhile, enhanced the adhesion between films and substrates.

1. Introduction

In the past years, semiconductor metal sulfides, especially CdS, PbS, ZnS, CuS and CoS, have caught extensive attention because of their attractive physical and chemical properties for the potential applications in many fields.[1-4] In particular, copper sulfides (Cu_xS, x = 1-2) have aroused considerable interests due to their variations in stoichiometric composition, valence states, complex structures, and different unique properties.[5-7] Copper sulfides have different stoichiometric forms, including at least five stable phases at room temperature: covellite (CuS) at the copper-deficient side, anilite ($Cu_{1.75}S$), digenite ($Cu_{1.8}S$), djurleite ($Cu_{1.97}S$), and chalcocite (Cu_2S) at the copper-rich side.[8-11] Copper sulfides with different stoichiometries show prospective applications in solar cells, photocatalysis, photo-thermal conversion, sensors, lithium rechargeable batteries and etc.[12-16] Significantly, copper sulfides, owing to their low cost, environmental friendliness and various band-gap energies in a range of 1.2-2.0 eV, are considered as one of the most promising materials for the future sustainable energy supply.[17, 18]

Recently, the fine control of nanomaterials with versatile chemical composition, crystal structure, size shape and surface chemistry has attracted increasing attention, mainly due to their ability to modulate the optical, electronic and catalytic response of materials, and then show important technological applications as advanced materials with unique properties.[19-21] Copper sulfides with various morphologies, such as nanoplates,[20] nanosheets,[22] hollow spheres,[3] nanoparticles,[23-25] nanowires,[21, 26, 27] tubular structure,[28] flower-like,[29, 30] hierarchical nanostructures,[8, 31, 32] and etc., have been obtained via many synthesis routes, including successive ionic layer adsorption and reaction (SILAR) method,[2] wet chemical bath,[13] sol-gel method,[9, 19] hydrothermal or solvothermal process,[33, 34] mechanical alloying and spark plasma sintering technique,[14] chemical vapor deposition,[35, 36] atomic layer deposition,[37] microemulsion approach,[11] and an in situ template-controlled method.[38] For example, Kim et al. used single-crystalline wurtzite CdS nanowires underwent gas-phase substitution to form unique superlattice cubic $Cu_{1.8}S$ and hexagonal Cu_2S nanowires through thermal evaporation of $CuCl_2$ at 500-600 °C.[26] Feldmann et al. prepared CuS, $Cu_{1.8}S$ and Cu_2S hollow spheres via a microemulsion route by adjusting the experimental conditions.[11] Xu et al. chose Cu_2O crystals with various well-defined morphologies, such as cubic, octahedral and star-like shapes, as the sacrificial templates to prepare copper sulfide materials, which could be tuned from Cu_2S to $Cu_{1.75}S$ by controlling the reaction conditions from N_2 to air atmosphere, respectively.[38] However, there are few reports about the synthesis of copper sulfide nanostructures directly grown on conductive substrates to simplify the preparation process of electrodes.

In this regard, fluorine-doped tin oxide (FTO) glasses were deposited with CuS seeds by spin coating method and subsequently set in Teflon-lined autoclaves only containing thiourea, $Cu(NO_3)_2$ ethanol solution as precursor to grow CuS nanosheet arrays on the pre-treated FTO substrates. When using CuCl as the copper source, rough $Cu_{1.8}S$ nanosheet films were successfully developed from the seeded FTO substrates. Since copper sulfides are regarded as one of the most efficient counter electrode materials in QDSSCs, it was found that the as-prepared CuS and $Cu_{1.8}S$ nanosheets had superior electrocatalytic activity for the reduction of polysulfide electrolyte than the conventional Pt films, which in turn reflected enhanced power conversion efficiencies of QDSSCs.

2. Experimental Section

2.1 Fabrication of CuS and $Cu_{1.8}S$ nanosheet arrays.

The FTO substrate (F:SnO_2, 0.5 cm × 1.2 cm) was ultrasonically cleaned for 15 min in a mixed solution of acetone and ethanol (v/v, 1:1), followed by deionized water rinsing for 15 min. CuS seeds were planted on the cleaned FTO substrate via spin coating by alternating 0.01 M $Cu(NO_3)_2$ and 0.01 M Na_2S aqueous solution for three times. The seeded FTO substrate was

placed in a Teflon-lined stainless steel autoclave (50 mL) containing 40 mL ethanol with 0.05 M $Cu(NO_3)_2$ and 0.1 M thiourea. The solvothermal reaction was performed at 150 °C for 24 h in an oven. When the autoclave was cooled to room temperature, the FTO substrate was taken out, rinsed with ethanol, and dried in air. Then, CuS nanosheet arrays grown on FTO substrate were obtained. For $Cu_{1.8}S$ nanosheet film, CuCl was alternatively employed as the copper source in the similar solvothermal reaction.

2.2 Preparation of CdS/CdSe QDSSCs.

For QDSSCs, hierarchical TiO_2 spheres reported in our previous work were used as the photoanode material.[39] The photoanode films with thickness about 20 μm were obtained by coating the hierarchical TiO_2 sphere paste on FTO glasses using doctor blade method. After a calcination process at 450 ^oC for 30 min to remove the organic substances, the TiO_2 films were soaked in 0.2 M $TiCl_4$ aqueous solution at 70 ^oC for 40 min followed by calcining at 450 ^oC for 30 min.

To fabricate CdS/CdSe QDSSCs, CdS and CdSe QDs deposited onto the TiO_2 photoanodes was realized by the chemical bath deposition (CBD) technique in refrigerator with temperature under 10 °C.[40] CdS QDs was deposited in an aqueous solution containing 20 mM $CdCl_2$, 66 mM NH_4Cl, 140 mM thiourea, and 230 mM ammonia (pH = 9.5) for 80 min. The deposition of CdSe QDs was subsequently carried out in a mixture of Na_2SeSO_3 solution and 0.08 M $Cd(NO_3)_2$ solution with a volume ratio of 1:1 for 30 h. The used Na_2SeSO_3 aqueous solution was prepared by dissolving Se (0.1 M) in an aqueous solution of Na_2SO_3 (0.18 M) at 70 ^oC for about 7 h when the black Se powder was almost reacted. After cooling to room temperature, the obtained Na_2SeSO_3 aqueous solution was filtered to remove unreacted Se powder.

CdS/CdSe sensitized TiO_2 films with an active area of about 0.20 cm^2 were assembled together with the above-prepared CEs by applying a 60 μm thick hot-melt sealed film as the spacer (SX1170-25; Solaronix Co.). The polysulfide electrolyte used here consists of 3.5 mL DI water and 1.5 mL methanol with 0.5 M Na_2S, 0.125 M S and 0.2 M KCl. The electrolyte was injected between two electrodes and driven by capillary force through the hole on the hot-melt sealed film.[16, 41]

2.3 Characterization

The morphology of samples were observed by field emission scanning electron microscopy (FESEM, HITACHI S-4800) and transmission electron microscopy (TEM, JEOL JEM-2100) with an accelerating voltage of 200 kV. Phase identification of materials was examined by X-ray diffraction (XRD, Panalytical X'pert PRO). The X-ray photoelectron spectroscopy (XPS) analysis was carried out with Quantum 2000 Scanning ESCA Microprobe spectrometer using a focused monochromatized Al Kα radiation (1486.6 eV). Performance of the as-prepared DSSCs was achieved by measuring photocurrent density-photovoltage (*J-V*) curves under AM 1.5G simulated solar light (Oriel 300 W Xe lamp and Newport AM-1.5G filter). The incident-photon-to-current efficiency (IPCE) spectra as a function of wavelength (λ = 300 to 800 nm) were measured by a monochromator (Oriel, Model: 74125). Cyclic voltammogram (CV) was carried out on the Autolab electrochemical workstation in a three-electrode system with counter electrodes as the working electrodes, a Pt foil as the counter electrode, and an SCE electrode as the reference electrode at a scan rate of 50 mV s^{-1}. The electrolyte was 70 mL DI water and 30 mL methanol with 0.5 M Na_2S, 0.125 M S and 0.2 M KCl. The charge transfer resistance was determined by electrochemical impedance spectra (EIS), performed on the symmetric cells using the Autolab electrochemical workstation under open circuit voltage (0 V) over a frequency range from 10^5 to 10^{-1} Hz with an AC voltage magnitude of 10 mV. The impedance data were analyzed by Autolab electrochemical EIS fitting software. The electrochemical workstation was also employed to measure the Tafel-polarization curves of the symmetric cells at a scan rate of 5 mV s^{-1}.

3. Results and Discussion

As shown in Fig. 1a, XRD pattern revealed that CuS (JCPDS No. 06-0464) film was obtained via solvothermally treating the seeded FTO substrate in the ethanol containing 0.05 M $Cu(NO_3)_2$ and 0.1 M thiourea at 150 °C for 24 h. The product had XRD diffraction peaks at 2θ = 27.1°, 27.6°, 29.2°, 31.7°, 32.8°, 47.9° and 59.3°, corresponding with those of lattice planes (100), (101), (102), (103), (006), (110) and (116) of hexagonal CuS phase. In addition, if change copper source in the reaction solution from $Cu(NO_3)_2$ to CuCl, under the same solvothermal condition, the resulting product can be indexed to $Cu_{1.8}S$ (JCPDS No. 24-0061) with diffraction peaks observed at 2θ = 27.7°, 32.1°, 46.1° and 54.6°, associating with those of lattice planes (111), (200), (220) and (311) of cubic $Cu_{1.8}S$ phase (Fig. 1b). Since the CuS and $Cu_{1.8}S$ films were thin (~ 1 μm), then the XRD signals of FTO substrates were strong (Fig. 1).

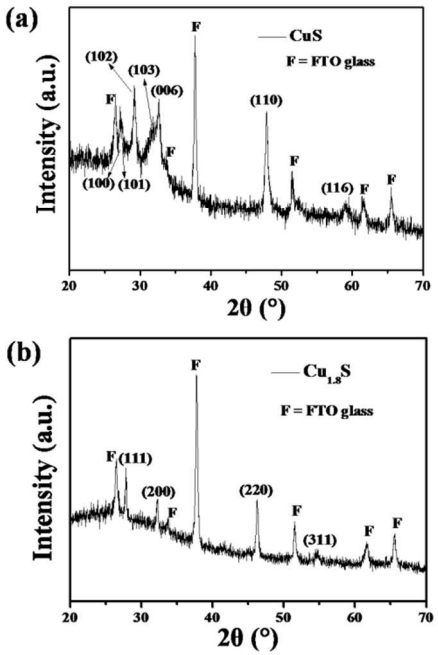

Fig. 1 XRD patterns of (a) CuS and (b) $Cu_{1.8}S$ nanosheet films prepared via solvothermal process.

Fig. 2 shows SEM images of the CuS and $Cu_{1.8}S$ films indexed by XRD patterns in Fig. 1. As shown in Fig. 2a and 2b, the CuS film consisted of well-defined nanosheet arrays, and the vertical CuS nanosheets randomly intercrossed with each other and well uniformly grew on the FTO substrate. It was observed that such CuS nanosheets were smooth with a thickness of about 10 nm (Fig. 2b). For $Cu_{1.8}S$ film, similar nanosheet arrays were successfully planted on the FTO substrate (Fig. 2c and 2d). Compared to CuS nanosheets (Fig. 2b), $Cu_{1.8}S$ nanosheets were relatively rough with a thickness of around 50 nm (Fig. 2d).

Obviously, the type of copper salt used in the solvothermal reaction played a heavy impact on the shape and crystal phase of products.

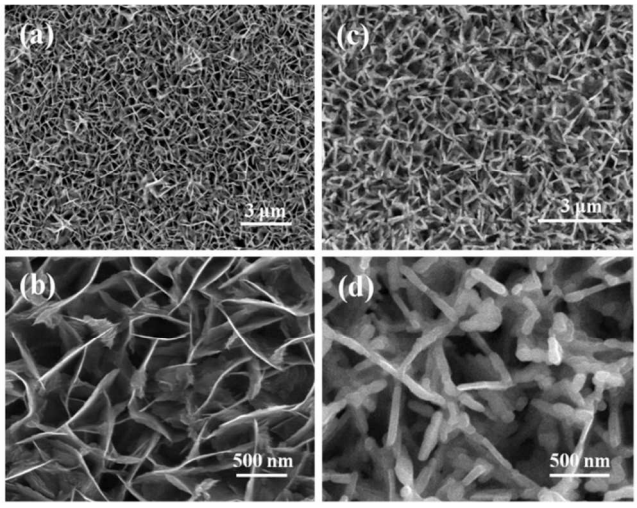

Fig. 2 SEM images of (a) CuS and (c) $Cu_{1.8}S$ nanosheet films; (b) and (d) are the magnified images of (a) and (d), respectively.

To further study the detailed structures of products, TEM measurement was subsequently performed. The obtained TEM images also revealed that the CuS nanosheet had smooth surface (Fig. 3a), while the $Cu_{1.8}S$ nanosheet was rough (Fig. 3c). These two types of nanosheets were both completely crystalline as proved by the HRTEM images (Fig. 3b and 3d). Lattice fringes with interplanar spacing, d_{102} = 0.304 nm (Fig. 3b) and d_{200} = 0.279 nm (Fig. 3d) can be indexed to hexagonal CuS phase and cubic $Cu_{1.8}S$ phase, respectively. The corresponding SAED patterns (insets in Fig. 3b and 3d) of the CuS and $Cu_{1.8}S$ nanosheets demonstrated that they were single crystals with great crystallinity. In addition, the corresponding EDX results were showed in Fig.S1. The ratios of Cu and S atoms for CuS and $Cu_{1.8}S$ nanosheets were 1.002:1 and 1.787:1, respectively, which were almost the same as 1:1 and 1.8:1.

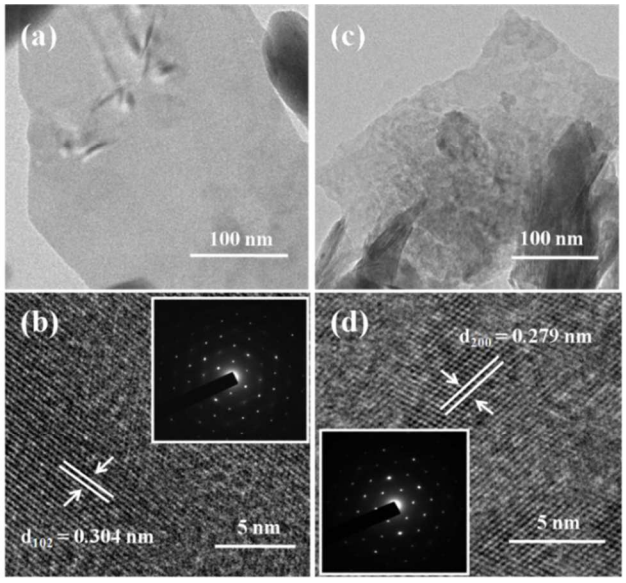

Fig. 3 TEM and HRTEM images of (a, b) CuS and (c, d) $Cu_{1.8}S$ nanosheet films, insets are the corresponding SAED patterns of (b) and (d), respectively.

XPS analysis was carried out to investigate the chemical binding states of the as-prepared CuS and $Cu_{1.8}S$ nanosheets. Fig. 4a exhibits the XPS spectrum of Cu 2p for CuS nanosheets. Two main peaks locating at 931.9 and 951.9 eV (Fig. 4a) were assigned to Cu $2p_{3/2}$ and Cu $2p_{1/2}$, respectively. Moreover, there were weak shake-up satellite peaks at around 943 eV (rectangle marked in Fig. 4a), suggesting the presence of paramagnetic chemical state of Cu^{2+}.[42] The corresponding XPS spectrum of S 2p for CuS nanosheets was shown in Fig. 4b. In the case of the XPS spectrum of Cu 2p for $Cu_{1.8}S$ nanosheets, the Cu $2p_{3/2}$ and Cu $2p_{1/2}$ peaks were observed at 932.1 and 952.1 eV (Fig. 4c), respectively. Noticeably, the accompanying Auger line (Cu LMM) at 568.6 eV (inset in Fig. 4c) indicated that the Cu ion was in the form of Cu (I) state, implying that the chemical binding state of $Cu_{1.8}S$ was close to Cu_2S.[42] Also, Fig. 4d shows the corresponding XPS spectrum of S 2p for $Cu_{1.8}S$ nanosheets.

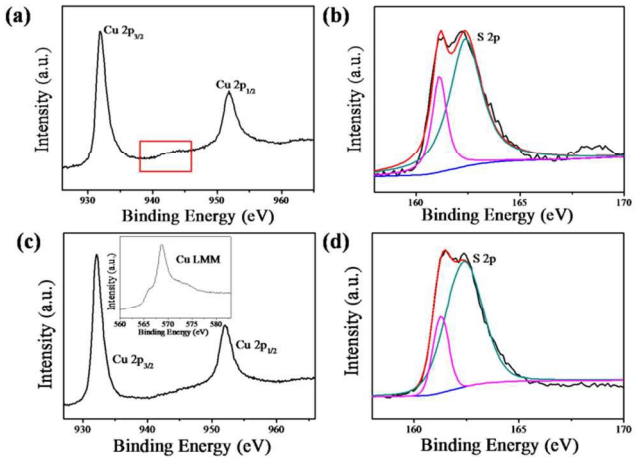

Fig. 4 The high resolution XPS spectra of Cu 2p and S 2p: (a, b) CuS and (c, d) $Cu_{1.8}S$ nanosheet films, inset in (c) is the Auger Cu LMM spectrum in the Cu LMM region for $Cu_{1.8}S$ sample.

In the control experiments, it was found that the CuS seeds on FTO substrates promoted the successful growth of copper sulfide nanosheet arrays. If the FTO substrate was absent of seeding treatment, after solvothermal reaction in ethanol containing the same precursor, not film was formed and only some microsphere products dispersed on the FTO substrate (Fig. S2a). If employing drop cast method to prepare CuS seeds on the FTO substrate, a CuS nanosheet film was obtained after the same solvothermal reaction (Fig. S2b). However, the quality of such CuS nanosheet film was poor. Then, CuS seeds prepared via spin coating led to the successful fabrication of vertical copper sulfide nanosheet arrays with high quality as shown in Fig. 2. In addition, the adjusting of solvothermal conditions, such as precursor concentration (Fig. S3a), reaction temperature (Fig. S3b and S4a) and growth time (Fig. S4b), remarkably influenced the features of copper sulfide nanosheet arrays.

Table 1 Performance parameters of the QDSSCs based on Pt, CuS and $Cu_{1.8}S$ counter electrodes, and results of the EIS fitting using the electrical equivalent circuit model in Fig. 6c.

Sample	J_{sc} (mA cm^{-2})	V_{oc} (V)	*FF*	*PCE* (%)	R_s (Ω)	R_{CT} (Ω)
Pt	13.31	0.50	0.30	1.99	6.21	1836
$Cu_{1.8}S$	16.07	0.50	0.41	3.30	6.11	44.34
CuS	15.08	0.51	0.51	3.95	6.53	33.36

The CuS and $Cu_{1.8}S$ nanosheet arrays grown on FTO substrates (Fig. 2) were then applied as counter electrodes (CEs) to assemble CdS/CdSe QDSSCs (Experimental Section). Table 1 summarizes the photovoltaic parameters of the resulting QDSSCs and Fig. 5a shows the corresponding current-voltage (*J-V*) characteristics. Using the Pt CE-based QDSSC as reference, largely enhanced photovoltaic performance of the QDSSCs employing CuS and $Cu_{1.8}S$ nanosheets as CEs was finally obtained (Table 1). In comparison with Pt CE, CuS and $Cu_{1.8}S$ nanosheet CEs endowed the cells with higher short circuit current density (J_{sc}; Pt: 13.31 mA cm^{-2} vs. $Cu_{1.8}S$: 16.07 mA cm^{-2} and CuS: 15.08 mA cm^{-2}) and fill factor (*FF*; Pt: 0.30 vs. $Cu_{1.8}S$: 0.41 and CuS: 0.51), and thus obviously improved power conversion efficiency (*PCE*; Pt: 1.99% vs. $Cu_{1.8}S$: 3.30% and CuS: 3.95%) for the assembling QDSSCs. Therefore, it was indicated that these CuS and $Cu_{1.8}S$ nanosheet arrays had better electrocatalytic ability for the polysulfide reduction. In addition, CuS nanosheet arrays exhibited relatively higher *PCE* value than that of $Cu_{1.8}S$ nanosheet arrays for the corresponding QDSSCs; this was probably because the crystal phase of CuS nanosheets matched well with that of CuS seeds, and then the CuS nanosheet film with fewer structure defects had better contact with the FTO substrate. However, the rough $Cu_{1.8}S$ nanosheets had slightly higher J_{sc} value partially since they owned larger surface areas to give more catalytic sites for the polysulfide reduction. Furthermore, we also prepared the Cu_2S/brass CE and its corresponding QDSSC. As shown in Fig.S5a, the cell efficiency of Cu_2S/brass CEs can be up to 3.12%, but it quickly decreased to 0.65% after 1-2 hours because of the exfoliation of Cu_2S film from brass. For other kinds of CEs, after several tests, CuS and $Cu_{1.8}S$ CEs showed relatively higher stability as compared to Pt and Cu_2S CEs (Fig.S5).

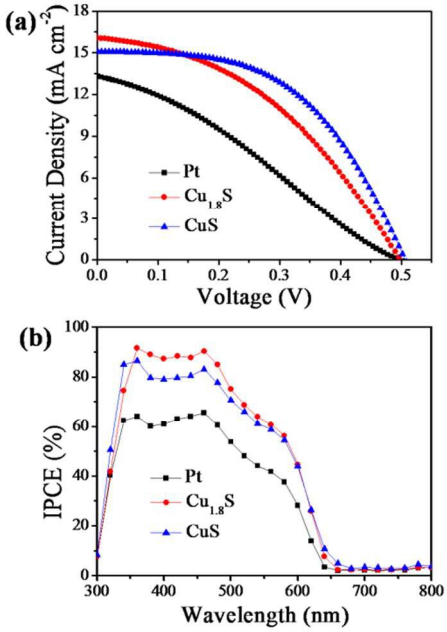

Fig. 5 (a) *J-V* curves and (b) *IPCE* spectra of the QDSSCs based on Pt, CuS and $Cu_{1.8}S$ counter electrodes.

Fig. 5b shows the incident photon-to-current efficiency (IPCE) spectra measured to scrutinize the different photovoltaic performance of the QDSSCs based on Pt, $Cu_{1.8}S$ and CuS CEs. The IPCE spectra of $Cu_{1.8}S$ and CuS-based QDSSCs were both higher over almost the tested wavelength region (300–800 nm) as compared to Pt-based QDSSC; moreover, $Cu_{1.8}S$-based QDSSC was slightly higher than CuS-based QDSSC. The IPCE results agreed well with the aforementioned J_{sc} values of the three QDSSCs (Table 1). The improved J_{sc} values of $Cu_{1.8}S$ and CuS-based QDSSCs were mainly attributed to their greater electrocatalytic ability for the polysulfide reduction, which was further confirmed by the following electrochemical analysis, namely, cyclic voltammetry (CV), electrochemical impedance spectroscopy (EIS) and Tafel polarization measurements.

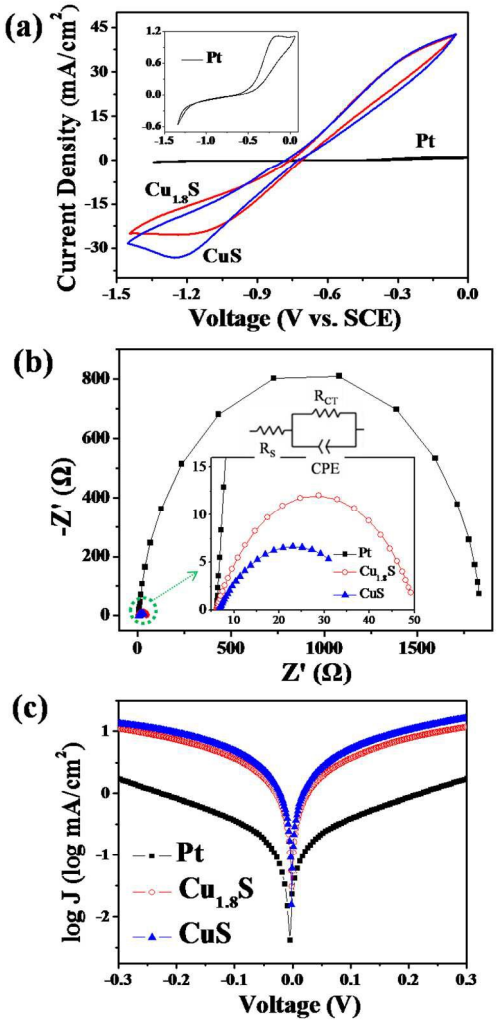

Fig. 6 Electrochemical characterization of the three counter electrodes in a three-electrode system with SCE used as reference: (a) Cyclic voltammogram of Pt, CuS and $Cu_{1.8}S$ electrodes in a mixture of methanol and DI water (3/7, v/v) containing 0.5 M Na_2S, 0.2 M S, and 0.2 M KCl; inset is the magnified cyclic voltammogram of Pt counter electrode from (a). (b) EIS plots, top inset is the electrical equivalent circuit model and bottom inset is the enlarged Nyquist plot of the part marked with green cycle, and (c) Tafel curves of the symmetric cells based on Pt, CuS and $Cu_{1.8}S$ counter electrodes.

The CV analysis was applied to investigate the electrochemical electrocatalytic activity of these three electrodes. Generally, the negative currents of CV plots represent the reduction of S_x^{2-} ions to S^{2-} ions while their positive currents are related to the oxidation of S^{2-} ions in the polysulfide electrolyte. As the CE materials in QDSSCs, the reduction peak currents of CV plots for the electrodes directly reflect the electrocatalytic ability of the CEs for S_x^{2-} reduction.[43] Accordingly, the $Cu_{1.8}S$ and CuS nanosheet electrodes (Fig. 6a) with consumedly higher

current densities at the reduction peaks of CV plots in comparison with Pt electrode (inset in Fig. 6a) had superior electrocatalytic ability for S_x^{2-} reduction. Meanwhile, CuS electrodes with better crystal structure exhibited a relatively higher reduction peak current than that of $Cu_{1.8}S$ electrodes.

Furthermore, Fig. 6b exhibits the EIS spectra of symmetric cells organized by Pt, $Cu_{1.8}S$ and CuS CEs, respectively. After fitting the experiment data via the equivalent circuit (inset in Fig. 6b), the resulting Nyquist plots of EIS spectra showed one semicircles which was associated with the charge-transfer resistance (R_{CT}) and interfacial capacitance (CPE) at the CE/electrolyte interface.[44] As shown in Table 1, the R_{CT} value of Pt CE was very large, confirming its poor electrocatalytic activity in polysulfide electrolyte. CuS electrode had smaller R_{CT} value than that of $Cu_{1.8}S$ electrode, which was mainly because the formed CuS nanosheets had fewer structure defects and better contact with FTO substrate.

In addition, Tafel-polarization analysis was performed using the same symmetric cells in the above EIS measurement. As showed in Fig. 6c, the Tafel polarization curve is the logarithmic current density (log J) as a function of the voltage (V). The exchange current density (J_o) of samples can be evaluated as the intercept of the extrapolated linear region of anodic and cathodic branches when the voltage is zero. Moreover, the J_o also can be calculated by the equation of $J_o = RT/nFR_{CT}$.[45, 46] Therefore, the higher J_o value, the lower R_{CT} value. It was observed that CuS electrode had the highest J_o value with the lowest R_{CT} value, suggesting the best electrocatalytic activity in well agreement with the CV and EIS results.

4. Conclusion

Seed assisted-solvothermal process has been firstly exploited to develop vertical CuS and $Cu_{1.8}S$ nanosheet arrays directly grown on FTO substrates. The type of copper salt used in the solvothermal reaction remarkably influenced the crystal phases and features of the resulting products. The obtained CuS and $Cu_{1.8}S$ nanosheet arrays exhibited enhanced *PCEs* up to 3.95% and 3.30% when used as CEs in QDSSCs, implying increases of 98% and 66% as compared to Pt-based QDSSC, respectively. Such synthesis strategy not only simplified the preparation procedure of CEs, but also achieved efficient QDSSC devices based on the formed copper sulfide CEs.

Acknowledgements

The authors gratefully acknowledge the financial supports from the National Basic Research Program of China (2012CB932900), and the National Natural Science Foundation of China (21321062).

Notes and references

[a]*Research Institute for Soft Matter and Biomimetics, School of Physics and Mechanical & Electrical Engineering, Xiamen University, Xiamen, 361005, China*

[b]*State Key Laboratory of Physical Chemistry of Solid Surfaces, and Department of Chemistry, College of Chemistry and Chemical Engineering, Xiamen University, Xiamen, 361005, China*

[*]*To whom correspondence should be addressed. Email: cjlin@xmu.edu.cn*

†Electronic Supplementary Information (ESI) available: FESEM images of copper sulfide films prepared in other control experiments.

1. L. Bakueva, I. Gorelikov, S. Musikhin, X. S. Zhao, E. H. Sargent and E. Kumacheva, *Adv. Mater.* , 2004, **16**, 926-929.
2. N. Balis, V. Dracopoulos, K. Bourikas and P. Lianos, *Electrochim. Acta* 2013, **91**, 246-252.
3. J. Gao, Q. Li, H. Zhao, L. Li, C. Liu, Q. Gong and L. Qi, *Chem. Mater.* , 2008, **20**, 6263-6269.
4. W. Guo, C. Chen, M. Ye, M. Lv and C. Lin, *Nanoscale*, 2014, **6**, 3656-3663.
5. I. Grozdanov and M. Najdoski, *J. Solid State Chem.* , 1995, **114**, 469-475.
6. Q. Lu, F. Gao and D. Zhao, *Nano Lett.* , 2002, **2**, 725-728.
7. X. L. Yu, C. B. Cao, H. S. Zhu, Q. S. Li, C. L. Liu and Q. H. Gong, *Adv. Funct. Mater.* , 2007, **17**, 1397-1401.
8. B. Li, Y. Xie and Y. Xue, *J. Phys. Chem. C* 2007, **111**, 12181-12187.
9. X. Zheng, Z. Jin, H. Liu, Y. Wang, X. Wang and H. Du, *Appl. Surf. Sci.* , 2013, **266**, 39-45.
10. W. Georg, E. Hinze and A. R. M. Abdelrahman, *Eur. J. Mineral.* , 2002, **14**, 591-598.
11. P. Leidinger, R. Popescu, D. Gerthsen, H. Lünsdorf and C. Feldmann, *Nanoscale*, 2011, **3**, 2544-2551.
12. M.-C. Lin and M.-W. Lee, *Electrochem. Commun.* , 2011, **13**, 1376-1378.
13. M. Basu, A. K. Sinha, M. Pradhan, S. Sarkar, Y. Negishi and T. Pal, *Environ. Sci. Technol.* , 2010, **44**, 6313-6318.
14. Z.-H. Ge, B.-P. Zhang, Y.-X. Chen, Z.-X. Yu, Y. Liu and J.-F. Li, *Chem. Commun.* , 2011, **47**, 12697-12699.
15. H. Lee, S. W. Yoon, E. J. Kim and J. Park, *Nano Lett.* , 2007, **7**, 778-784.
16. M. Ye, C. Chen, N. Zhang, X. Wen, W. Guo and C. Lin, *Adv. Energy Mater.*, 2014, **4**, 1301564.
17. L. Isac, A. Duta, A. Kriza, S. Manolache and M. Nanu, *Thin Solid Films* 2007, **515**, 5755-5758.
18. Y. Wu, C. Wadia, W. Ma, B. Sadtler and A. P. Alivisatos, *Nano Lett.* , 2008, **8**, 2551-2555.
19. X. Liu, X. Wang, B. Zhou, W. C. Law, A. N. Cartwright and M. T. Swihart, *Adv. Funct. Mater.* , 2012, **23**, 1256–1264.
20. P. Kumar, M. Gusain and R. Nagarajan, *Inorg. Chem.* , 2011, **50**, 3065-3070.
21. H.-X. Zhang, J.-P. Ge, J. Wang and Y.-D. Li, *Nanotechnology*, 2006, **17**, S253.
22. Y. Lei, H. Jia, Z. Zheng, Y. Gao, X. Chen and H. Hou, *CrystEngComm*, 2011, **13**, 6212-6217.
23. W. Li, A. Shavel, R. Guzman, J. Rubio-Garcia, C. Flox, J. Fan, D. Cadavid, M. Ibáñez, J. Arbiol and J. R. Morante, *Chem. Commun.* , 2011, **47**, 10332-10334.
24. H. Zhang, Y. Zhang, J. Yu and D. Yang, *J. Phys. Chem. C* 2008, **112**, 13390-13394.
25. Z. Zhuang, Q. Peng, B. Zhang and Y. Li, *J. Am. Chem. Soc.* , 2008, **130**, 10482-10483.
26. H. S. Kim, T. K. Sung, S. Y. Jang, Y. Myung, Y. J. Cho, C.-W. Lee, J. Park, J.-P. Ahn, J.-G. Kim and Y.-j. Kim, *CrystEngComm*, 2011, **13**, 2091-2095.
27. P. Roy and S. K. Srivastava, *Crystal Growth & Design*, 2006, **6**, 1921-1926.
28. X. Zheng and Q. Hu, *Appl. Phys. A* 2009, **94**, 805-812.
29. Z. Nan, X.-Y. Wang and Z. Zhao, *J. Cryst. Growth* 2006, **295**, 92-96.
30. A.-M. Qin, Y.-P. Fang, H.-D. Ou, H.-Q. Liu and C.-Y. Su, *Crystal Growth & Design*, 2005, **5**, 855-860.
31. F. Li, W. Bi, T. Kong and Q. Qin, *Cryst. Res. Technol.* , 2009, **44**, 729-735.
32. J. Xu, X. Yang, T.-L. Wong and C.-S. Lee, *Nanoscale*, 2012, **4**, 6537-6542.
33. L. Ge, X.-y. Jing, J. Wang, S. Jamil, Q. Liu, D.-l. Song, J. Wang, Y. Xie, P.-p. Yang and M.-l. Zhang, *Crystal Growth & Design*, 2010, **10**, 1688-1692.

34. Y. Zhao, H. Pan, Y. Lou, X. Qiu, J. Zhu and C. Burda, *J. Am. Chem. Soc.* , 2009, **131**, 4253-4261.
35. J. P. Ge, J. Wang, H. X. Zhang and Y. D. Li, *Chem. Eur. J.* , 2004, **10**, 3525-3530.
36. M. Xu, H. Wu, P. Da, D. Zhao and G. Zheng, *Nanoscale*, 2012, **4**, 1794-1799.
37. L. Reijnen, B. Meester, F. de Lange, J. Schoonman and A. Goossens, *Chem. Mater.* , 2005, **17**, 2724-2728.
38. S. Jiao, L. Xu, K. Jiang and D. Xu, *Adv. Mater.* , 2006, **18**, 1174-1177.
39. M. Ye, C. Chen, M. Lv, D. Zheng, W. Guo and C. Lin, *Nanoscale*, 2013, **5**, 6577-6583.
40. X.-F. Guan, S.-Q. Huang, Q.-X. Zhang, X. Shen, H.-C. Sun, D.-M. Li, Y.-H. Luo, R.-C. Yu and Q.-B. Meng, *Nanotechnology*, 2011, **22**, 465402.
41. M. D. Ye, X. K. Xin, C. J. Lin and Z. Q. Lin, *Nano Lett.* , 2011, **11**, 3214-3220.
42. M. Lee and K. Yong, *Nanotechnology*, 2012, **23**, 194014.
43. J. G. Radich, R. Dwyer and P. V. Kamat, *J. Phys. Chem. Lett.* , 2011, **2**, 2453-2460.
44. Y. Yang, L. Zhu, H. Sun, X. Huang, Y. Luo, D. Li and Q. Meng, *ACS Appl. Mater. Interfaces* 2012, **4**, 6162-6168.
45. J. Dong, S. Jia, J. Chen, B. Li, J. Zheng, J. Zhao, Z. Wang and Z. Zhu, *J. Mater. Chem.* , 2012, **22**, 9745–9750.
46. W. Guo, Y. Shen, M. Wu, L. Wang and T. Ma, *Chem. Eur. J.* , 2012, **18**, 7862-7868.

Cite this: DOI: 10.1039/ c1ee00000x

www.rsc.org/ees

PAPER

The table of contents entry

In Situ Growth of CuS and $Cu_{1.8}S$ Nanosheet Arrays as Efficient Counter Electrodes for Quantum Dot-Sensitized Solar Cells

By *Meidan Ye,[a] Xiaoru Wen,[b] Nan Zhang,[b] Wenxi Guo,[a] Xiangyang Liu,[a] Changjian Lin*[ab]*

Keywords: CuS and $Cu_{1.8}S$ nanosheet arrays, seed-assisted solvothermal processing, quantum dot-sensitized solar cells (QDSSCs).

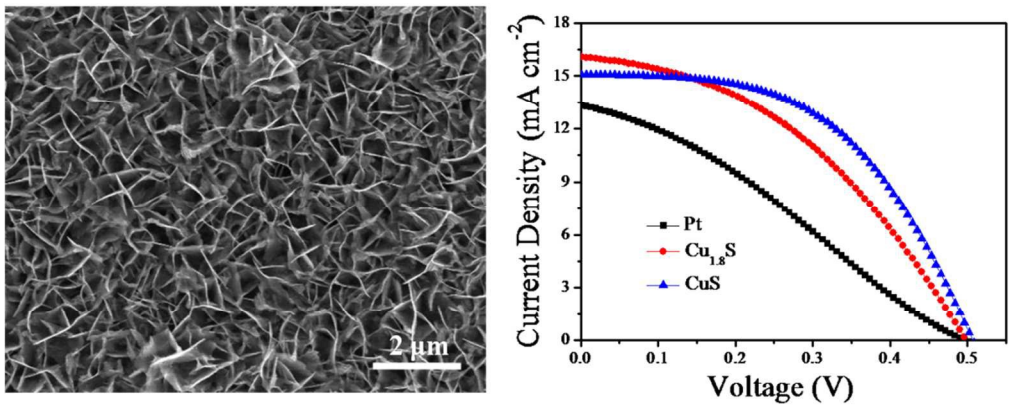

Vertical CuS and $Cu_{1.8}S$ nanosheet arrays directly grown on conductive substrates were successfully developed via a seed-assisted solvothermal processing. Upon the QDSSC application, such novel structure-based counter electrodes exhibited superior performance with a maximum increase of 98% as compared to conventional Pt counter electrodes.